geomatics

MDPI

Article

Qualitative Model for Hurricane-Induced Debris Flow Prediction: A Case Study of the Impact of Hurricane Maria (2017) in Puerto Rico

Yuri Gorokhovich [1,*], Ivan V. Morozov [2], Günay Erpul [3], Chia-Ying Lee [4], Carolynne Hultquist [5] and Zola Qingyang Yin [6]

[1] Lehman College, City University of New York, Bronx, NY 10468, USA
[2] City College, City University of New York, New York, NY 10017, USA; imorozo000@citymail.cuny.edu
[3] Department of Soil Science and Plant Nutrition, Faculty of Agriculture, Ankara University, 0600 Ankara, Türkiye; erpul@ankara.edu.tr
[4] Ocean and Climate Physics, Lamont-Doherty Earth Observatory (LDEO), Columbia University, New York, NY 10027, USA; cl3225@columbia.edu
[5] School of Earth and Environment, University of Canterbury, Christchurch 8041, New Zealand; carolynne.hultquist@canterbury.ac.nz
[6] Fu Foundation School of Engineering & Applied Science, Columbia University, New York, NY 10027, USA; qy2307@columbia.edu
* Correspondence: yuri.gorokhovich@lehman.cuny.edu

Abstract

This study applies a qualitative Geographic Information Systems model that integrates satellite-derived wind and rainfall data to predict potential debris-flow locations in Puerto Rico triggered by Hurricane Maria (2017). A key innovation of the model is the use of wind-driven rainfall (WDR), calculated at multiple elevation levels using satellite wind data and Global Precipitation Measurement (GPM) precipitation at three time steps. WDR replaces the conventional use of total rainfall commonly applied in landslide modeling. A second innovation is the use of WDR slope exposure to hurricane direction in place of a standard aspect parameters. The model assumes that WDR was the primary trigger of debris flows during the hurricane. Predicted debris-flow locations were compared with mapped debris-flow inventories using threshold distances of 1000, 500, and 250 m. Prediction rates ranged from 30 to 100%, and success ratios from 10 to 90%, depending on elevation and distance thresholds, with the best performance at 500 and 1000 m ranges. Model performance could be enhanced through higher-resolution satellite observations of wind, soil moisture, and precipitation, supporting potential real-time hazard applications. Model limitations include its empirical nature, qualitative structure, and current applicability to equatorial or sub-equatorial regions affected by hurricanes or typhoons. Further testing and regional calibration are recommended.

Keywords: landslides; debris flows; GIS; hurricanes; prediction

Academic Editor: Enrico Corrado Borgogno Mondino

Received: 25 November 2025
Revised: 29 January 2026
Accepted: 3 February 2026
Published: 5 February 2026

1. Introduction

Landslide predictions are complicated because of the natural variability of environmental parameters and the shortage of high-quality data for validation. Predictive methods range from physical modeling [1] to logistic regression [2], from neural network [3] to machine learning [4,5], and models based on threshold values [6,7] or probabilistic methods [8].

Many predictive models use landslide inventories [9,10] to test the prediction of inventoried locations or newly occurred landslides in order to produce landslide susceptibility maps.

Landslide types and triggers vary, ranging from debris flows caused by intensive rainfall impact on weathered sediments to rotational landslides caused by excessive soil moisture or slope destabilization by anthropogenic factors or natural causes, as well as creep caused by soil structure, and rockfalls caused by earthquakes or slope destabilization. All of these combinations of potential parameters make landslide predictive models diverse and complex in nature. The selection of methods depends on specific landslide type and trigger; however, regardless of the landslide type and triggers, many existing models are time-demanding in terms of implementation and producing results. This makes it difficult to develop operational real-time landslide predictive models for providing a forecast within a few hours of landslide event occurrence.

In this paper, we focus on a very specific landslide type -a debris flow and a specific trigger—hurricane/typhoon. This is a very common combination in tropical and subtropical areas where strong hurricanes/typhoons induce intensive geologic weathering, setting conditions for debris flows. Operational qualitative real-time landslide models can be used for preparedness and mitigation efforts, and to provide timely information to people to make decisions. We concentrate on the Caribbean and Central America regions where for the period 2004–2013, there were 611 landslides recorded that caused 11,631 deaths due to the hurricane's impact [11]. This analysis indicates heavy rainfall and other hurricane impacts as factors contributing to fatalities, especially fatal landslides.

To date, there are no operational real-time predictive landslide models used in the Caribbean and Central American countries. Some US-based early warning systems were designed for rainfall-triggered landslides [12] and are based on historical landslide data and thresholds of the rainfall that help identify the probability of landslide occurrence. A system developed by Fengjia (Feng Chia) from the University Geographic Information System Research Center provides landslide data in real-time to users [13]. This application (https://246.ardswc.gov.tw (Accessed on 27 January 2026)) helped users to see maps with potential landslides triggered by typhoon Gaemi (Kemi) that hit Taiwan in July 2024. Predictions in this system are derived from pre-compiled 1420 creeks and downstream areas prone to debris flows and inundation database (IPDB) based on hydrologic model HEC-1. As the site was still active at the time of preparing this article, we were not able to ascertain its performance.

A recent rainfall-triggered landslide application is a global real-time awareness system called LHASA (Landslide Hazard Assessment for Situational Awareness), developed by NASA [14] to "provide situational awareness of landslide hazards in near real-time". This system is based on real-time data from the Global Precipitation Measurement (GPM) satellite system and Global Landslide Catalog (GLC) [15]. The triggering rainfall in this model is computed by antecedent rainfall index (ARI) based on the last seven days of rainfall. ARI weighting was calibrated by 949 landslides from the years 2007–2013. LHASA is a step forward in global landslide awareness in real-time to help users to see potentially affected areas based on GPM, GLC, and ARI data; however, the system cannot be used as an operational real-time hurricane-induced landslide prediction tool since it does not show specific landslide locations and serves mainly as an awareness system.

We propose an innovative approach towards the development of an operational predictive model of landslides, specifically debris flows, caused by hurricanes. The method uses the interaction between rotating cyclonic water mass and terrain aspect [16,17] to estimate wind-driven rainfall (WDR) and its impact. The verification of the model was made possible through public availability of landslide data collected by low-altitude aerial photography after hurricanes Stan (2005), Maria (2017), and Mitch (1998) [18–20]. This data

presents a unique opportunity for research as all of the mapped landslides were triggered by hurricanes, whereas many landslide inventories contain records of landslides caused by multiple triggers in different years without attribution to a specific trigger or event time.

The research goal of this paper is to present a simple and replicable prototype methodology for operational real-time hurricane-induced landslide prediction. The novelty of the methodology is the ability to show potential landslide locations before or during the hurricane, relative to the time of satellite observation, alongside terrain characteristics and elevation ranges, i.e., in both temporal and spatial scales. As a case study for calibration and verification, we chose Hurricane Maria (2017) in Puerto Rico; for additional verification of the model, we used cases of Hurricanes Mitch (1998) and Stan (2005) in Guatemala and Honduras (Figure 1) [18–20].

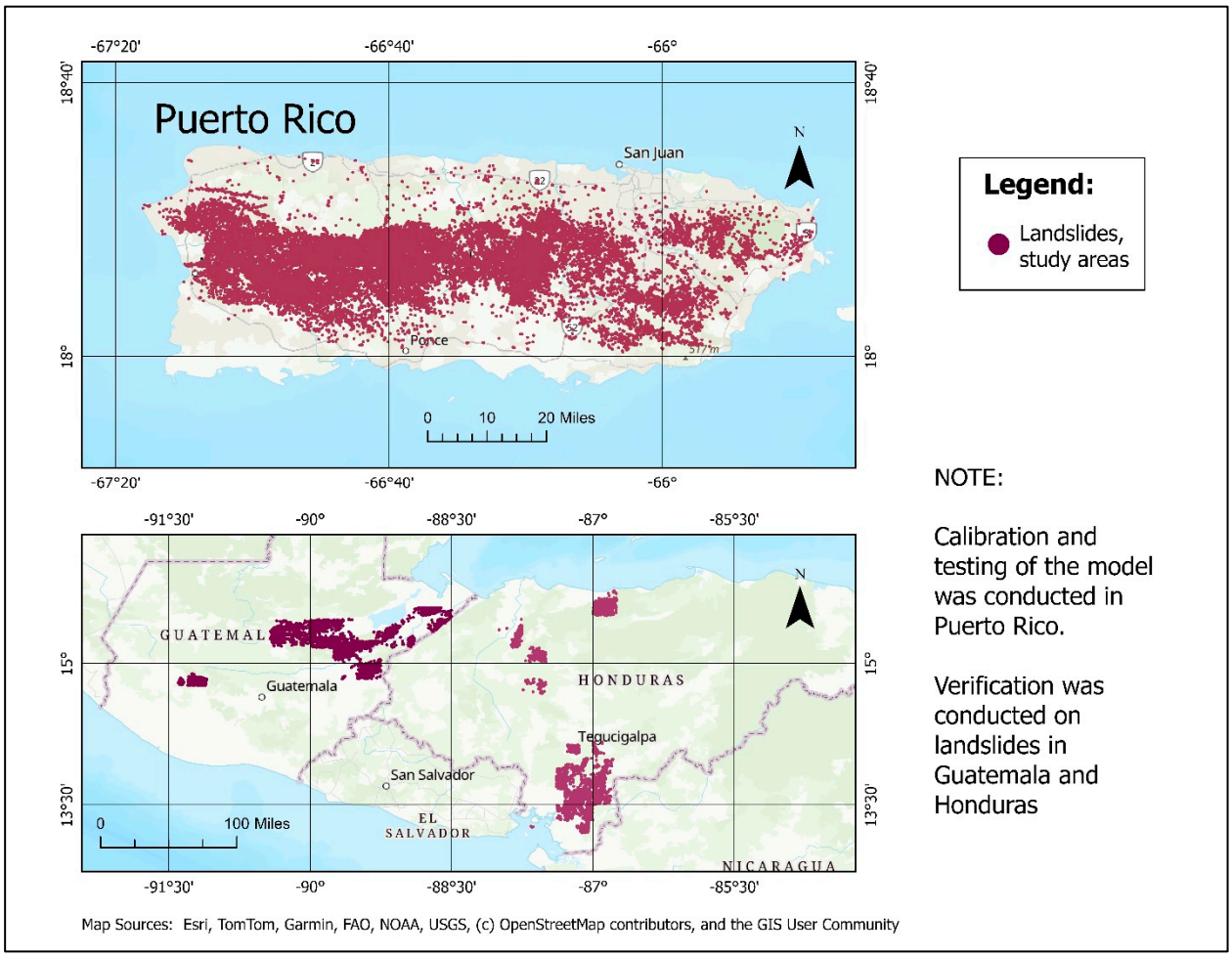

Figure 1. Study area. Coordinate system: WGS84.

2. Methodology and Data

2.1. Proposed Model Characteristics

The core of the modeling is based on so-called wind-driven rainfall (WDR) caused by hurricanes/typhoons and its interaction with the aspect and slope of the terrain. The following are the main assumptions underlying the modeling process:

1. In tropical and subtropical areas, geologic substrate is heavily weathered due to the regular hurricane/typhoon impact over thousands of years. Therefore, the surface material is crumbled and loose, thus creating a base for debris flows, which is a typical landslide type in Central America, the Caribbean basin, and south-eastern

Asia. Debris flows are triggered primarily by the high moisture content and can reach 2 m in depth [21]. Specifically, for assessment of the impact of Hurricane Maria [22], authors underlined that "bedrock geology alone did not determine the location and distribution of landslides caused by Hurricane Maria. While rainfall data collected during Hurricane Maria were inconsistent, satellite-based soil moisture data were correlated with the distribution of landslides." Upon completion of the assessment, the authors concluded that landslide densities were not controlled by geologic formations but variable soil moisture.

2. Rainfall from hurricanes/typhoons is not vertical due to their cyclonic structure. Therefore, the rainfall impact in the model is considered from WDR and not direct vertical rainfall. WDR can be higher or lower, depending on the terrain slope and wind velocity and can be calculated from satellite data for various elevation levels.
3. The aspect of the terrain is one of the most important modeling parameters due to the impact of the WDR on windward slopes and its lower (or no) impact on the leeward (or downwind) slopes. This effect is similar to the well-known orographic effect. A study by Larsen and Torres Sánchez (1992) [21] shows the distribution of landslides in the Luquillo Experimental Forest in Puerto Rico during Hurricane Hugo (1989) on the predominant terrain aspect, impacted by the hurricane path and direction, and coinciding with 61% of the landslides. Similar results are described in [17].
4. In our model, we prioritize geomorphologic and meteorological factors of landslide susceptibility as opposed to vegetation and geology. The importance of the selected factors is highlighted in [23] and the Kirschbaum, Stanley, and Simmons (2015) study of the landslide hazard assessment system for Central America and Hispaniola [24].

A flowchart of the modeling methodology and its structure is depicted in Figure 2.

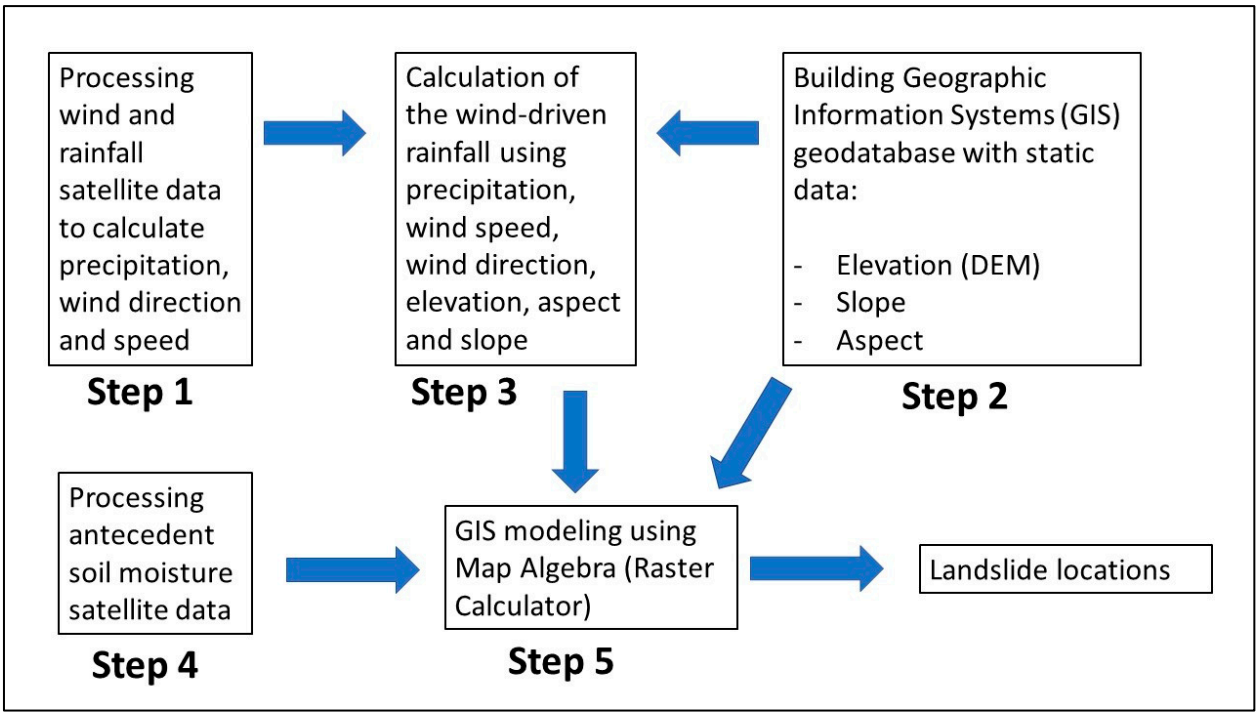

Figure 2. Flowchart of the modeling procedure. All spatial processing was performed using ArcGIS Pro 3.4 (ESRI, Inc., Redlands, CA, USA).

The model brings together satellite-derived inputs and static GIS data on the terrain. GIS is used to process and calculate a new raster dataset with potential landslides locations.

Landslides mapped and digitized after Hurricane Maria were used later for calibration and verification purposes.

2.2. Data

All meteorological data used in the model are in the public domain from NASA portals EARTHDATA and GES DISC. Elevation data, aspect, and slope were derived from the NASA Shuttle Radar Topography Mission Global 1 arc second. Soil moisture data were obtained from the Soil Moisture Active Passive (SMAP) satellite mission stored with the National Snow and Ice Data Center (NSIDC). Mapped landslides after Hurricanes Maria, Stan and Mitch were obtained from [18–20].

2.2.1. Meteorological Data

Wind and precipitation data collected by NASA are as follows: Modern-Era Retrospective Analysis for Research and Applications, Version 2 (MERRA2), and Global Precipitation Measurement (GPM) of product with Integrated Multi-Satellite Retrievals for GPM (IMERG, version 7). Wind speed, wind direction, and precipitation rate were derived from this data (see methodology in [16]) and used in WDR calculation for four daily intervals (12 a.m., 6 a.m., 12 p.m., and 6 p.m.) and 72 model-levels (pressures/elevation levels) specified in documentation [25]. Since Hurricane Maria left Puerto Rico by midnight of 20 September, we used only 6 a.m., 12 p.m., and 6 p.m. intervals. It is highly likely that major landslide events occurred during these periods.

MERRA2 data include wind components U (eastward) and V (northward), obtained from the Meteorological Operational Satellite-A (MetOp-A) ASCAT and WindSat [25]. Both components are available in instantaneous data with frequency 6 h from 00:00 UTC and model-level (elevation) levels 1–72. Model-level data in MERRA2 and corresponding terrain elevations are in Table S1. Because the highest elevation in Puerto Rico is Cerro de Punta at 1338 m, and our comparative studies in Guatemala and Honduras do not exceed 4200 m, Table S1 contains values only up to level 53 = 4204.7 m a.s.l. In real time, for operational use, the MERRA2 data can be replaced with global weather prediction systems such as the Global Forecast System (GFS) from the National Oceanic and Atmospheric Administration (NOAA) National Centers for Environmental Prediction (NCEP), or its higher-resolution hurricane forecast model—the Hurricane Analysis and Forecast System (HAFS).

Rainfall half-hour IMERG data were aggregated by six-hour intervals to correspond to the temporal resolution of MERRA2 data. The spatial resolution of IMERG data is approximately 10.5 km [26].

2.2.2. Geomorphologic and Soil Moisture Datasets

Table S2 contains descriptions and sources of the geomorphologic and soil datasets used in modeling.

2.3. Landslide Prediction Process

Our modeling process was conducted in stages using four Python 3.9 scripts for automation:

1. Wind and precipitation data processing using IMERG and MERRA2 data;
2. WDR calculation;
3. Prediction;
4. Testing and verification.

2.3.1. Wind and Precipitation Data Processing

Wind data (MERRA2) were downloaded from the NASA portal and a Python script converted the original NetCDF file (.nc) into a raster layer in ArcGIS Pro (ESRI Inc.). The script extracts also V and U wind components to calculate wind direction and speed. The methodology is described at length in [16]. Precipitation data (IMERG, v.7) were similarly downloaded and Python script converted NetCDF files (.nc) into raster layers in ArcGIS Pro (ERSI, Inc.) and combined them according to 6 h temporal resolution of MERRA2 data.

2.3.2. Wind-Driven Rainfall (WDR) Calculation: Methodology and Justification

Wind-driven rainfall (WDR) represents the effective component of oblique precipitation acting on sloped terrain under strong winds. During hurricanes, rainfall rarely falls vertically; instead, the cyclonic wind field produces intense horizontal momentum that drives raindrops at an angle, enhancing rainfall impact and infiltration on windward slopes while reducing it on leeward slopes. This process significantly contributes to slope saturation, pore-pressure buildup, and debris-flow initiation [27–29]. Consequently, WDR serves as a physically meaningful proxy for the spatial variability of rainfall forcing and one of the most critical predictors in our debris-flow susceptibility model.

(a) Physical background. Laboratory rainfall–wind tunnel experiments [27,28] demonstrated that the kinetic energy of raindrop impact and rain splash detachment increase non-linearly with the angle of incidence and wind speed. Under high-velocity wind regimes, the rainfall vector tilts toward the slope surface, concentrating rainfall energy flux along windward aspects. In hurricane environments, this obliquity transforms vertical rainfall intensity into a lateral driving component capable of intensifying soil wetting, disaggregation, and shallow failure. Our model thus substitutes the conventional vertical rainfall rate (from IMERG) with WDR, calculated as a function of both wind magnitude and wind–slope orientation.

(b) Computational formulation. Our innovation to the original formula [30] in the WDR calculation was the inclusion of elevation level and time derived from satellite data; therefore, WDR estimation was done for each elevation level and three time intervals (06:00, 12:00, 18:00 UTC) using the modified formulation from [30,31] as follows:

$$\mathrm{WDR(lev, time)} = \sum Pv\,[1 + \tan a \tan b \cos(za - zb)] \quad (1)$$

where

WDR(lev, time)—wind-driven rainfall for a specific elevation level (lev) and time interval (time);

Pv—vertical precipitation (mm h^{-1}) from IMERG aggregated to 6 h intervals; total catch by a conventional horizontally oriented rain gauge for any time interval of interest;

a—terrain gradient (slope, rad);

b—angular departure of rainfall from the vertical;

za—terrain aspect (azimuth, °);

zb—hourly wind direction (azimuth, °) derived from MERRA-2 U-V components;

The angular rainfall departure b was computed by the arctangent interpolation:

$$b = \tan^{-1}(U/4.29) \quad (2)$$

where U is wind speed (m s^{-1}). The arctangent ensures a physically consistent upper limit of 90°, unlike polynomial fits previously used for moderate wind speeds [29]. This modification preserves geometric realism under extreme hurricane winds and facilitates stable extrapolation across elevation levels.

(c) Spatial and temporal integration. For each 30 m terrain pixel, WDR was calculated by combining IMERG precipitation, MERRA-2 wind components, and topographic slope/aspect. Although the spatial resolution of MERRA-2 (≈66 km) is coarser than the DEM, the angular alignment between wind vectors and terrain facets, rather than wind magnitude itself, governs WDR variability. Therefore, the method retains physical validity for estimating windward vs. leeward contrasts even under resolution mismatch. Future operational implementation can substitute MERRA-2 with finer-scale forecasts (e.g., NOAA GFS/HAFS).

2.3.3. Prediction

To translate continuous WDR fields into potential debris-flow initiation location, a qualitative raster-based Boolean model was used in GIS software ArcGIS Pro (ESRI, Inc) using a Python script. A terrain pixel was classified as a predicted landslide location when

1. WDR > 2× Vertical Rainfall (from IMERG, GPM);
2. Slope $\geq 9^{\circ}$;
3. Soil Moisture $\geq$ 0.45 Vol/vol;
4. Aspect Within $\pm 1^{\circ}$ of Hurricane Wind Direction;
5. Elevation Corresponds to the Analyzed Model Level.

These thresholds were calibrated empirically using 50% of mapped landslides from Hurricane Maria (training dataset, N = 35,710). WDR and soil-moisture parameters were adjusted manually with a goal to predict the number of landslides corresponding to the to the number of landslides in the training dataset. We started with low numbers and while increasing them, we were measuring the number of predicted vs. mapped landslides. The slope value represents a threshold greater than (mean—one standard deviation), based on the statistical distribution of the slope data from the total mapped landslides. This helped us to keep values that are within 1σ below the mean and above and to eliminate relatively low outliers.

2.3.4. Testing and Verification

To facilitate model testing and verification, we divided mapped landslides from Hurricane Maria in Puerto Rico in two subsets: one for testing/training and one for verification. The total number of mapped landslides is 71,420. This number was divided by half using a random selection tool (random number generator) "Subset Features" from ArcGIS Pro Geostatistical Analyst to create separate training and verification datasets. Specific thresholds of parameters in the qualitative GIS raster binary model were obtained during model training.

Verification of the landslide prediction results is difficult to assess, because while experimentally we can predict landslides and map them on terrain, in practice it is almost impossible to pinpoint their location and time due to the heterogeneity of the triggering factors and complexity of the geomorphological conditions. However, it is possible to use spatial proximities or tessellation to assess how close predictive locations are in relation to mapped landslides; therefore, the testing and verification script uses mapped landslides and verifies predicted landslides on the basis of their closest proximities.

We started with a tessellation method by creating a regular 1 km grid and experimented with the assessment of results by comparing the number of predicted and mapped landslides in each 1 km pixel. However, this method proved to be biased because grid boundaries divided clusters of landslides disproportionately. For example, adjacent grid pixels could have one pixel with few mapped landslides and no predicted, but the other pixels with many predicted and none mapped. This pixel would be counted as a "failed" prediction, though mapped landslides could be found within a 1 km distance or less.

Because of the biased nature of the "grid" method, we used another spatial method based on threshold distances (1000, 500 and 250 m) between mapped and modeled landslides by calculating the nearest distances between them. For each proximity threshold and for each elevation level, we identified the number of predicted landslides (i.e., for each mapped landslide, is there a modeled landslide within a certain proximity away? If yes, it is predicted), number of correct predictions (i.e., for each modeled landslide, is there a mapped landslide within a certain proximity away? If yes, it is a correct prediction), total number of mapped landslides, total number of predicted landslides, prediction (hit) rate (i.e., the ratio between the number of predicted landslides and the number of mapped landslides), and success ratio (i.e., the ratio between the number of correct predictions and the number of predicted landslides). For detailed information on prediction rate and success ratio calculations, see [32].

Quantitative performance of the modeling results was evaluated using F1 score, defined as the harmonic mean of precision and recall, usually used to evaluate the overall predictive skill of the model [33]. Although generalized formulations account for prevalence and bias in imbalanced datasets, the standard F1 definition was adopted here to provide a balanced and interpretable measure of model performance. F1 score was calculated using the following formula:

$$F1 = 2 \times (\text{Precision} \times \text{Recall})/(\text{Precision} + \text{Recall}) \quad (3)$$

where

F1—F1 score [33];
Precision—Success Ratio [32];
Recall—Prediction Rate [32].

3. Results

Our predictive model produced a set of expected landslide locations (points). Figures S1–S9 show mapped and predicted landslide distribution by elevation levels from MERRA2 wind data. Predicted landslides are shown as blue points while those observed through mapping are shown as red points.

Results were assessed by prediction (hit) rate and success ratio, which are both based on proximities between mapped and predicted landslides and their quantities. Figure S10 shows estimated assessment parameters (prediction rate and success ratio) for each studied case.

Quantitative Performance Summary

Prediction rate (recall) and success ratio (precision) mean values are derived from elevation-level data shown in Figures S1–S9, with the F1 score indicating balanced model skill; this data is summarized in Table S3.

4. Discussion

Quantitative evaluation of model performance (Table S3) demonstrates that the proposed WDR-based framework reproduces the spatial distribution of observed debris flows with satisfactory robustness across all proximity thresholds. Prediction rate (recall) and success ratio (precision) for the Hurricane Maria case exhibit the highest and most balanced values within the 500–1000 m range, signifying an optimal trade-off between detection capability and false-alarm reduction. At 250 m, performance metrics decline due to positional uncertainty associated with the spatial mismatch between MERRA-2 atmospheric inputs and high-resolution terrain data, which is a limitation typical of mixed-resolution modeling environments. The stability of precision and recall across intermediate thresholds indicates

that the model effectively captures the dominant geomorphological and meteorological controls of hurricane-induced landslides, validating its potential for near-real-time regional forecasting and early-warning applications.

Because of the availability of the soil moisture data (SMAP satellite mission) for the pre-Maria hurricane period, we were able to include it in the model for Puerto Rico as an antecedent soil moisture condition. For other cases (Hurricane Mitch in Honduras and Guatemala, and Hurricane Stan in Guatemala), we did not have this data because at that time they were not collected by NASA (SMAP was launched in 2015). Also, for the Hurricane Mitch cases, we had to digitize and interpolate precipitation data from available digital hard copy maps because no continuous precipitation data from satellites were available at that time. This could possibly cause poor prediction results for these cases.

We note a limitation in data integrated within the model as it features varying spatial resolution between high-resolution versus coarse data; our inputs range from 30 m (SRTM) to approximately 66 km (MERRA2). We acknowledge limited data as one of the deficiencies in the modeling process. NASA data does not provide better alternatives, yet the coarse inputs still provide useful timely context. While resampling can be applied, it does not add certainty. At this point, we do not claim spatial precision in our work, but reasonable accuracy of results, i.e., landslide locations within 500–1000 m threshold distances (Figure S1). Other layers could be introduced for future events to improve the spatial resolution.

The modeling algorithm used both vertical and temporal dimensions; however, we had to combine our temporal predictions for the day of hurricane impact because training and verification datasets did not have temporal variables since they were collected after the hurricane event.

Model testing was conducted using a training subset of the mapped landslides for Hurricane Maria, collected in Puerto Rico after the hurricane. During testing, we empirically modified parameters in the binary raster model and observed the proximity between predicted and mapped landslides in the training set as well as a balance between over and under prediction of landslide locations. These parameters were constant while testing the model performance for the Hurricane Mitch case in Honduras and Guatemala, and Hurricane Stan in Guatemala. There is an assumption that the surface geology structure in these countries is like Puerto Rico and debris flows are also the main hurricane impact.

Exclusively for Puerto Rico, we used a subset of the bedrock geology layer with geological units where no mapped landslides occurred: Tay, Tcbm and Ta; Tay—Aymamon Limestone; Tcbm—Montebello Limestone Member; Ta—Aguada Limestone [34]. These are strong bedrock formations that did not produce any debris flows during Hurricane Maria. However, because our results are based on proximities, vast "landslide void" areas bring the bias toward estimation of prediction and success rate by increasing distances between modeled and mapped landslides surrounding the bedrock formation. Therefore, areas of these geologic units were excluded from the spatial extent of the modeling by "masking them out".

The concept of WDR introduces a physically grounded mechanism that reconciles the apparent mismatch between coarse atmospheric data and fine topographic detail. While MERRA-2 wind fields cannot capture micro-scale gusts, the large-scale angular distribution of hurricane winds relative to terrain orientation dictates the spatial asymmetry of rainfall impact. The model's satisfactory correspondence between predicted and observed debris-flow clusters within 500–1000 m thresholds supports the hypothesis that windward–leeward contrasts, rather than absolute rainfall magnitude, dominate landslide triggering under cyclonic conditions. Further refinement with high-resolution wind products and in situ pluviometric records will enhance both the temporal precision and quantitative reliability of WDR-based forecasting.

Since empirical models depend on geographic location and their regional settings, users can regionally recalibrate slope angle, WDR ratio, aspect, and soil moisture in the GIS module of the model. This can be achieved by collecting high-resolution data on locations of landslides after hurricane impact. Then GIS components of the model should undergo sensitivity analysis by consequent change in each parameter, i.e., WDR ratio, slope, soil moisture, and aspect. By comparing the number of modeled and mapped landslides for each elevation level, the user can find the most appropriate thresholds.

4.1. Uncertainty and Limitations

Every real-time predictive framework that couples geomorphological and meteorological parameters inherits uncertainties from both data inputs and the process of representation. The present model is no exception and its outcomes should be interpreted within these constraints:

(a) Spatial resolution mismatch. A principal limitation arises from the different spatial scales of the input datasets—MERRA-2 meteorological grids (~66 km) and terrain-based geomorphological variables (30 m). This mismatch can introduce positional errors in the computed WDR field. However, since the model primarily exploits directional correspondence between wind vectors and terrain aspect rather than absolute wind magnitude, the large-scale angular coherence of hurricane winds largely preserves the physical realism of windward–leeward contrasts. Nevertheless, the approach would benefit from replacing MERRA-2 with higher-resolution products (e.g., GFS/HAFS or ERA5) as they become available for future events.

(b) Temporal uncertainty. Because mapped landslides were recorded only after the hurricane event, temporal validation of predicted initiation times was not possible. The model therefore represents spatial susceptibility snapshots for specific time intervals rather than continuous real-time sequences. Future versions could incorporate near-real-time soil-moisture retrievals and radar rainfall updates to improve temporal fidelity.

(c) Empirical threshold calibration. Thresholds used in the Boolean raster model (e.g., slope $\geq 9^{\circ}$, soil moisture ≥ 0.45, WDR $> 2\times$ vertical rainfall) were derived through empirical calibration. These values may vary with local lithology, vegetation cover, and storm intensity. Additional training datasets from other hurricanes will allow development of probabilistic or machine learning classifiers that provide confidence intervals instead of fixed cut-offs as well as algorithms for model calibration.

(d) Data completeness and mapping bias. Landslide inventories used for training and validation were compiled from aerial photography under post-event conditions. Inaccessible areas, cloud cover, and errors during landslide mapping [17] may have led to under-representation of smaller or shallow debris flows. Such omission errors likely contribute to the underestimation of prediction success ratios.

Despite these uncertainties, the model demonstrates consistent spatial agreement between predicted and mapped debris flow clusters within 500–1000 m thresholds. This suggests that, even with coarse atmospheric input, the WDR-driven framework captures the essential geomorphological controls of hurricane-induced mass movements. Continued refinement of data resolution, temporal updating, and probabilistic assessment will progressively transform the model from a qualitative diagnostic tool into an operational early-warning system.

4.2. Potential Operational Use of Modeling

While we cannot predict the exact landslide location due to the high heterogeneity of the geologic and meteorological factors and coarse resolution of the satellite measurements, the results of modeling were expressed as prediction (hit) rate and success ratio for three

threshold distances: 250, 500, and 1000 m. These thresholds help to identify "hot spots" (the most intensive expected landslide areas) that could be useful to operational use.

For "hot spot" evaluation, we selected the traditional GIS method known as Getis-Ord Gi statistics [35,36], based on neighborhood evaluation. This method works on point data and considers a distance factor. To check the method's applicability, we made a comparison between predicted and mapped "hot spot" analysis for the Hurricane Maria case in Puerto Rico. It showed that 97% of "hot spots" with confidence levels 90–99 based on modeled landslides match locations of the "hot spots" based on mapped landslides. This result is based on 500 m bin size and 1000 m neighborhood size in "hot spot" settings. Therefore, people in affected areas can receive real-time warning by viewing their location on the map to make an informed decision.

Figure 3 shows an example of the potential operational map with "hot spot" zones represented by 500 m squares. Areas categorized "Not Significant" still can have potential landslides. This should be considered in future applications of the model for landslide warnings, possibly by adding a warning for application users.

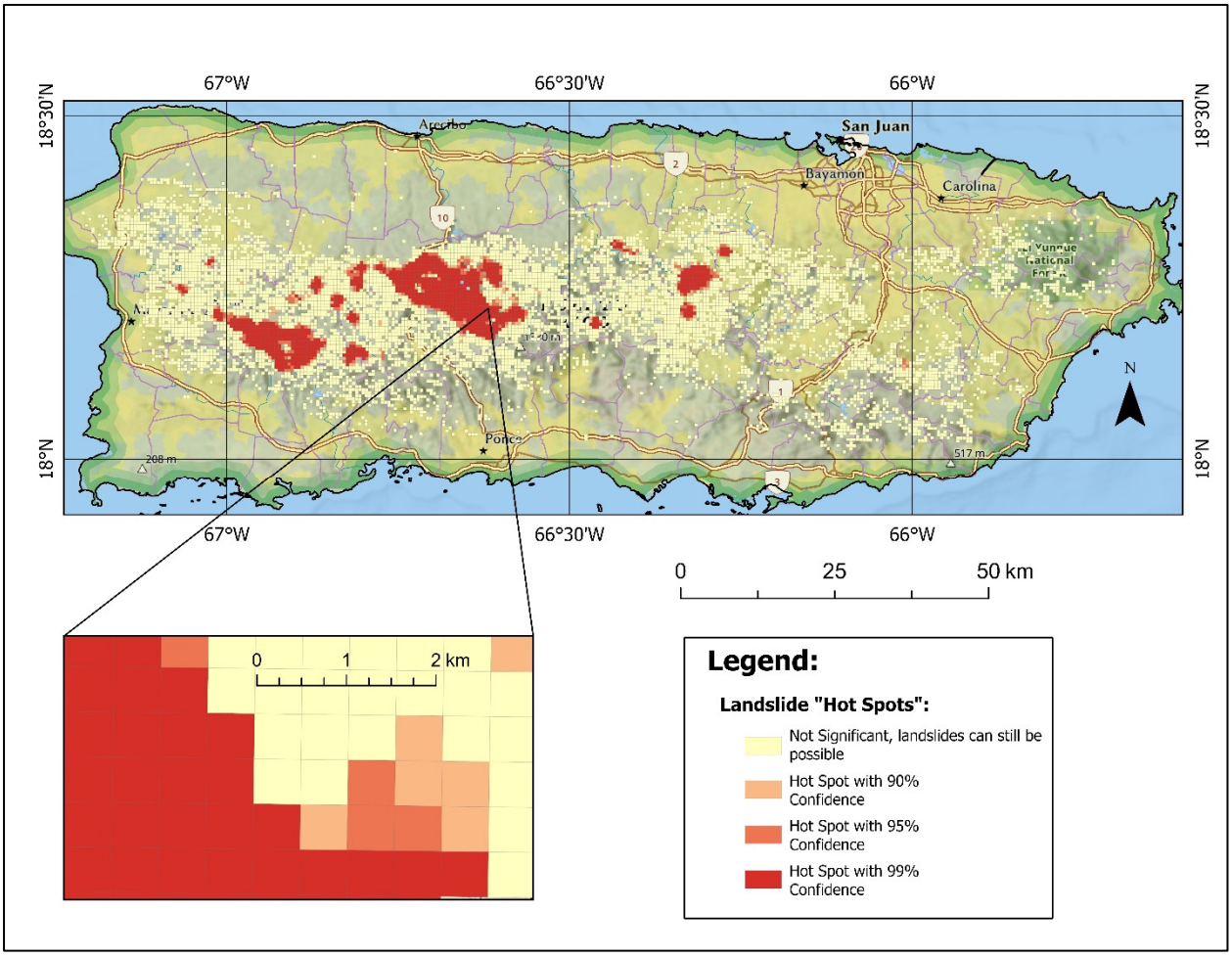

Figure 3. Results of landslide "hot spot" analysis with Getis-Ord Gi statistics. Coordinate system: WGS84.

5. Conclusions

1. Geomorphological characteristics of the terrain combined with meteorological data from hurricane events create a foundation for qualitative operational real-time landslide predictions. At this time, the best results (i.e., high prediction rates) are obtained

for the 500 and 1000 threshold distances, meaning that landslides will most likely occur within the area defined by these distances.

2. Real-time operational landslide prediction methodology can be run in real time to provide inhabitants of the affected areas with approximate locations of potential hazardous sites within hours before hurricane landfall. This can help to make decisions regarding evacuation, preparation, and/or landslide mitigation process.
3. Meteorological data from satellites provide unparalleled ability to predict landslide events in vertical and temporal dimensions.
4. Due to the coarse resolution of used satellite data, there is a need for NASA to improve spatial resolution of wind and soil moisture data to allow better integration of topographic, soil, and atmospheric data, eventually modeling results.
5. We found only a few mapped landslide databases publicly open for analysis. More landslide datasets, collected immediately after the hurricane, will help to improve models and expand the current effort to other areas of the world.

6. Future Potential

There are a few potential uses of the proposed model in operational real-time forecasting:

- Create a mobile app to inform users on hurricane conditions and potential locations of landslides in relation to the user's geographical location. An app could include essential information, such as the location of the nearest emergency shelter, contacts, hospitals, road conditions, and many other auxiliary information that can help users to make decisions.
- While the current model can predict landslide occurrences in two dimensions—vertical (elevation) and temporal (time)—we cannot verify it in the temporal dimension because mapped landslides were collected only after the hurricane, and not during the various time intervals of hurricane propagation. Therefore, there is a need for a geostationary satellite-based mapping system that could identify debris flows as soon as they occur at a high temporal resolution. This data will improve our forecasting and modeling abilities.
- With improvement in NASA satellite sensors, we can expect better temporal and spatial resolution on soil moisture data as well as wind data. This will allow landslide predictions at a finer granularity and improve the performance of models in the field.

Supplementary Materials: The following supporting information can be downloaded at https://www.mdpi.com/article/10.3390/geomatics6010015/s1; Table S1: Pressures and elevation for selected elevation levels in MERRA2 data (adapted from Table 4.2 in [25]); Table S2: Spatial datasets used in the landslide modeling; Figure S1: Results of modeling: predicted (blue) and observed (red) landslides at level 64. Coordinate system: WGS84; Figure S2: Results of modeling: predicted (blue) and observed (red) landslides at level 65. Coordinate system: WGS84; Figure S3: Results of modeling: predicted (blue) and observed (red) landslides at level 66. Coordinate system: WGS84; Figure S4: Results of modeling: predicted (blue) and observed (red) landslides at level 67. Coordinate system: WGS84; Figure S5: Results of modeling: predicted (blue) and observed (red) landslides at level 68. Coordinate system: WGS84; Figure S6: Results of modeling: predicted (blue) and observed (red) landslides at level 69. Coordinate system: WGS84; Figure S7: Results of modeling: predicted (blue) and observed (red) landslides at level 70. Coordinate system: WGS84; Figure S8: Results of modeling: predicted (blue) and observed (red) landslides at level 71. Coordinate system: WGS84; Figure S9: Results of modeling: predicted (blue) and observed (red) landslides at level 72. Coordinate system: WGS84; Figure S10: Success ratio and prediction (hit) rate at different elevation levels using different threshold distances; Table S3: Summary of model performance across three spatial proximity thresholds (250 m, 500 m, 1000 m) for all case studies.

Author Contributions: Conceptualization, Y.G.; methodology, Y.G., I.V.M. and G.E.; software, Y.G.; validation, Y.G., I.V.M. and C.-Y.L.; formal analysis, Y.G. and C.H.; investigation, Y.G. and Z.Q.Y.; resources, Y.G.; data curation, Y.G.; writing—original draft preparation, Y.G., G.E., C.-Y.L. and C.H.; writing—review and editing, C.H.; visualization, Y.G. and Z.Q.Y.; supervision, Y.G.; project administration, Y.G. All authors have read and agreed to the published version of the manuscript.

Funding: This research received no external funding.

Data Availability Statement: The raw data supporting the conclusions of this article will be made available by the authors on request.

Acknowledgments: Special thanks to the USGS for publicly distributing unique datasets on landslides for Puerto Rico after Hurricane Maria and for Honduras and Guatemala after Hurricanes Mitch and Stan, thus making this study possible.

Conflicts of Interest: The authors declare no conflicts of interest.

References

1. Sornette, D.; Helmstetter, A.; Andersen, J.V.; Gluzman, S.; Grasso, J.-R.; Pisarenko, V. Towards landslide predictions: Two case studies. *Phys. A Stat. Mech. Its Appl.* **2004**, *338*, 605–632. [CrossRef]
2. Brenning, A. Spatial prediction models for landslide hazards: Review and comparison. *Nat. Hazards Earth Syst. Sci.* **2005**, *5*, 853–862. [CrossRef]
3. Zhang, Y.; Tang, J.; He, Z.; Tan, J.; Li, C. A novel displacement prediction method using a gated recurrent unit model with time series analysis in the Erdaohe landslide. *Nat. Hazards* **2021**, *105*, 783–813. [CrossRef]
4. Li, H.; Xu, Q.; He, Y.; Deng, J. Prediction of landslide displacement using ensemble-based extreme learning machine and copula models. *Landslides* **2018**, *15*, 2047–2059. [CrossRef]
5. Krkač, M.; Špoljarić, D.; Bernat, S. Method for prediction of landslide movements based on random forests. *Landslides* **2017**, *14*, 947–960. [CrossRef]
6. Lee, J.H.; Kim, H.; Park, H.J.; Heo, J.H. Temporal prediction modeling for rainfall-induced shallow landslide hazards using extreme value distribution. *Landslides* **2021**, *18*, 321–338. [CrossRef]
7. Muntohar, A.S.; Mavrouli, O.; Jetten, V.G.; van Westen, C.J.; Hidayat, R. Development of a landslide early warning system based on satellite-derived rainfall thresholds in Indonesia. In *Understanding and Reducing Landslide Disaster Risk (WLF 2020)*; Casagli, N., Tofani, V., Sassa, K., Bobrowsky, P.T., Takara, K., Eds.; Springer: Cham, Switzerland, 2020. [CrossRef]
8. Jones, J.N.; Bennett, G.L.; Abancó, C.; Matera, M.A.M.; Tan, F.J. Multi-event assessment of typhoon-triggered landslide susceptibility in the Philippines. *Nat. Hazards Earth Syst. Sci.* **2023**, *23*, 1095–1115. [CrossRef]
9. Garcia-Urquia, E.; Axelsson, K. The use of press data in developing a database for rainfall-induced landslides in Tegucigalpa, Honduras. *Nat. Hazards* **2014**, *73*, 237–258. [CrossRef]
10. Guzzetti, F.; Mondini, A.C.; Cardinali, M.; Fiorucci, F.; Santangelo, M.; Chang, K.-T. Landslide inventory maps: New tools for an old problem. *Earth-Sci. Rev.* **2012**, *112*, 42–66. [CrossRef]
11. Sepúlveda, S.A.; Petley, D.N. Regional trends and controlling factors of fatal landslides in Latin America and the Caribbean. *Nat. Hazards Earth Syst. Sci.* **2015**, *15*, 1821–1833. [CrossRef]
12. Baum, R.L.; Godt, J.W. Early warning of rainfall-induced shallow landslides and debris flows in the USA. *Landslides* **2010**, *7*, 259–272. [CrossRef]
13. Hsu, M.H.; Chen, A.S.; Chen, L.C.; Lee, C.-S.; Lin, F.-T.; Huang, C.-J. A GIS-based Decision Support System for Typhoon Emergency Response in Taiwan. *Geotech. Geol. Eng.* **2011**, *29*, 7–12. [CrossRef]
14. Kirschbaum, D.; Stanley, T. Satellite-Based Assessment of Rainfall-Triggered Landslide Hazard. *Earth's Future* **2018**, *6*, 505–523. [CrossRef]
15. Kirschbaum, D.B.; Adler, R.; Hong, Y.; Hill, S.; Lerner-Lam, A. A global landslide catalog for hazard applications. *Nat. Hazards* **2010**, *52*, 561–575. [CrossRef]
16. Gorokhovich, Y.; Machado, E.A.; Giron Melgar, L.I.; Ghahremani, M. Improving landslide hazard and risk mapping in Guatemala using terrain aspect. *Nat. Hazards* **2016**, *81*, 869–886. [CrossRef]
17. Gorokhovich, Y.; Voustianiouk, A. Implications of slope aspect for landslide risk assessment: A case study of Hurricane Maria in Puerto Rico. *Geomorphology* **2021**, *391*, 107874. [CrossRef]
18. Machado, E.; Gorokhovich, Y.; Ghahremani, M. Landslide inventory dataset post Hurricane Stan (2005), Lake Atitlan region. *Data Brief* **2022**, *43*, 108356. [CrossRef]

19. Hughes, K.S.; Bayouth García, D.; Martínez Milian, G.O.; Schulz, W.H.; Baum, R.L. Map of slope-failure locations in Puerto Rico after Hurricane María. *US Geol. Surv. Data Release* **2019**, 672. [CrossRef]
20. Harp, E.L.; Hagaman, K.W.; Held, M.D.; McKenna, J.P. *Digital Inventory of Landslides and Related Deposits in Honduras Triggered by Hurricane Mitch*; U.S. Geological Survey: Reston, VA, USA, 2002.
21. Larsen, M.C.; Torres Sánchez, A.J. Landslides triggered by Hurricane Hugo in eastern Puerto Rico. *Caribb. J. Sci.* **1992**, *28*, 113–120.
22. Bessette-Kirton, E.; Cerovski-Darriau, C.; Schulz, W.H.; Coe, J.A.; Kean, J.W.; Godt, J.W.; Thomas, M.A.; Hughes, K.S. Landslides Triggered by Hurricane Maria: Assessment of an Extreme Event in Puerto Rico. *GSA Today* **2019**, *29*, 4–10. [CrossRef]
23. Menéndez-Duarte, R.; Marquínez, J.; Devoli, G. Slope instability in Nicaragua triggered by Hurricane Mitch. *Environ. Geol.* **2003**, *44*, 290–300. [CrossRef]
24. Kirschbaum, D.; Stanley, T.; Simmons, J. A dynamic landslide hazard assessment system for Central America and Hispaniola. *Nat. Hazards Earth Syst. Sci.* **2015**, *15*, 2257–2272. [CrossRef]
25. Bosilovich, M.G.; Lucchesi, R.; Suarez, M. *MERRA-2: File Specification; GMAO Office Note No. 9 (Version 1.1)*; NASA GSFC: Greenbelt, MD, USA, 2016; 73p.
26. Huffman, G.J.; Bolvin, D.T.; Joyce, R.; Kelley, O.A.; Nelkin, E.J.; Tan, J.; Watters, D.C.; West, B.J. *Integrated Multi-Satellite Retrievals for GPM (IMERG) Technical Documentation*; NASA Goddard Space Flight Center: Greenbelt, MD, USA, 2023.
27. Erpul, G.; Norton, L.D.; Gabriels, D. The Effect of Wind on Raindrop Impact and Rainsplash Detachment. *Trans. ASAE* **2002**, *45*, 51–62. [CrossRef]
28. Erpul, G.; Norton, L.D.; Gabriels, D. Raindrop-Induced and Wind-Driven Particle Transport. *Catena* **2002**, *47*, 227–243. [CrossRef]
29. Erpul, G.; Gabriels, D.; Cornelis, W.M.; Samray, H.N.; Guzelordu, T. Sand detachment under rains with varying angle of incidence. *Catena* **2008**, *72*, 413–422. [CrossRef]
30. Pike, R.J.; Sobieszczyk, S. Soil slip/debris flow localized by wind-driven rain in the San Francisco Bay region storm of January 1982. *Geomorphology* **2008**, *94*, 290–313. [CrossRef]
31. Guthrie, R.H.; Mitchell, S.J.; Lanquaye-Opoku, N.; Evans, S.G. Extreme weather and landslide initiation in coastal British Columbia. *Q. J. Eng. Geol. Hydrogeol.* **2010**, *43*, 417–428. [CrossRef]
32. Jolliffe, I.T.; Stephenson, D.B. *Forecast Verification: A Practitioner's Guide in Atmospheric Science*; Wiley: Hoboken, NJ, USA, 2012.
33. Powers, D.M.W. Evaluation: From precision, recall and F-measure to ROC, informedness, markedness and correlation. *Int. J. Mach. Learn. Tech.* **2011**, *2*, 37–63.
34. Bawiec, W.J. *Geology, Geochemistry, Geophysics, Mineral Occurrences, and Mineral Resource Assessment for the Commonwealth of Puerto Rico: Open-File Report 98-38*; U.S. Geological Survey: Reston, VA, USA, 1998.
35. Ord, J.K.; Getis, A. Local Spatial Autocorrelation Statistics: Distributional Issues and an Application. *Geogr. Anal.* **1995**, *27*, 286–306. [CrossRef]
36. Getis, A.; Ord, J.K. The Analysis of Spatial Association by Use of Distance Statistics. *Geogr. Anal.* **1992**, *24*, 189–206. [CrossRef]